

A Slice Puncturing Scheme of Energy Storage Batteries for Grid Frequency Regulation

Jian Feng, *Graduate Student Member, IEEE*, Hongxun Hui, *Senior Member, IEEE*,
Shaohua Yang, *Member, IEEE*, and Fen Hou, *Member, IEEE*

Abstract—Frequency deviations caused by renewable energy fluctuation and sudden load change pose significant threats to grid frequency stability. Energy storage batteries (ESBs), with their rapid ramp-up times and flexible control capabilities, have become ideal resources for grid frequency regulation. On one hand, wireless transmission technologies such as fifth-generation (5G) have been widely employed to transmit frequency regulation signals. On the other hand, wireless transmission faces the challenge of limited spectrum resources, which is related to grid frequency regulation performance. Hence, in spectrum-limited scenarios, how to allocate spectrum resources reasonably between ESBs and other grid users requires an in-depth investigation. In particular, exclusively reserving frequency resource for ESBs can achieve good frequency regulation performance (communication delay is low), but it significantly reduces spectrum efficiency since the frequency regulation signal is bursty traffic and exclusive reservation will need to resource waste. Conversely, allocating spectrum resources to ESBs only when needed can ensure higher spectrum efficiency, but lead to poor frequency regulation performance (communication delay is high with the best effort service). To address the above issue, we introduce a 5G slice puncturing technology, allowing ESBs to dynamically share spectrum resources with other grid users in spectrum-limited scenarios. In addition, we further design the puncturing scheme to ensure fair sharing among multiple ESBs during frequency regulation. Finally, our proposed scheme is validated in a frequency response model and the results indicate that the puncturing scheme improves by 22.8% in maximum frequency deviation (MFD).

Index Terms—frequency regulation, energy storage batteries, wireless transmission, spectrum-limited, 5G slice puncturing

NOMENCLATURE

Acronyms

ESB	Energy storage battery
5G	Fifth-generation
SC	Subcarrier
eMBB	Enhanced mobile broadband
URLLC	Ultrareliable low latency communications
QoS	Quality-of-service
BS	Base station

This work is supported in part by the Science and Technology Development Fund, Macau SAR (Project no. 001/2024/SKL, 0068/2023/RIB3, and 0062/2024/RIA1), in part by the project funded by University of Macau (Project no. MYRG-GRG2023-00200-FST and MYRG-CRG2024-00011-IOTSC), in part by the National Natural Science Foundation of China (Grant No. 52407075), and in part by the Guangdong Basic and Applied Basic Research Foundation, China (2025A1515011531). (Corresponding author: Fen Hou.)

J. Feng, H. Hui, S. Yang, and F. Hou are with the State Key Laboratory of Internet of Things for Smart City and Department of Electrical and Computer Engineering, University of Macau, 999078 Macao SAR (email: yc37939@um.edu.mo, hongxunhui@um.edu.mo, shaohuayang@um.edu.mo, fenhou@um.edu.mo).

PMU	Phasor measurement unit
CSI	Channel state information
RBG	Resource block group
DPP	Drift-plus-penalty
OTOM	One-to-one matching
USP	Universal slice puncturing
MFD	Maximum frequency deviation.
Variables and Parameters	
\mathbb{V}, v	Set and index of remote users
\mathbb{E}, e	Set and index of ESBs
\mathbb{M}, m	Set and index of RBGs
g_i, h^i	Channel power gain and small-scale fading of user i
d_i	Distance from BS to user i
φ	Path-loss exponent
N_0	Power spectral density of Gaussian white noise
r_v^M, r_e^B	Data rates for remote user v and ESB e
B_v^M, B_e^B	Used bandwidths of remote user v and ESB e
P_M, P_B	Transmit power of BS to remote users and ESBs
t	Index of the frame (time slot before Section IV)
T	System time
T_s	Duration of one frame
T_{tl}^e	Total delay of frequency regulation signal to ESB e
T_{PMU}	Time delay from PMU to control center
T_c	Transmission delay from control center to BS
T_b^e	Transmission delay from BS to ESB e
t_b^e	Sending time from BS to ESB e
t_q^e	Queuing time for ESB e
$Q_v(t)$	Queue backlog of remote user v at the t -th frame
$A_v(t)$	Arrival rate of remote user v at the t -th frame
$R_v(t)$	Departure rate of remote user v at the t -th frame
$G_v(t)$	Virtual queue of remote user v at the t -th frame
λ_v	Mean of Poisson distribution for remote user v
δ_v	Threshold of the queue backlog of remote user v
l_v	Delay requirement of remote user v
ω	Maximum delay violation probability for remote users
Ω_1	Total bandwidth resource usage for remote users
Ω_2	Upper bound of the DPP function
$I_{v,m}$	Indicator of RBG allocation between remote user v and RBG m
V_1, V_2	Control parameters in the DPP method
η_v	Number of RBG allocated to remote user v using OTOM algorithm
Δf	System frequency deviation
ΔP_L	System power load
ΔP_G	Power generation deviation
ΔP_B	Total power output of ESBs

T_g, T_t, T_r	Time constant of the speed governor, the turbine and the reheat process
F_{HP}	High-pressure turbine's power fraction
K, R	Proportional and integral gains
H, K_D	Generator inertia and load-damping factor
P_{rp}^e	Rated power of ESB e
W	Sum of the products of each ESB's total time delay and its rated power
k	Index of the slot in each frame, $k \in \{1, \dots, 10\}$
t_s	Sum of t_b^e within a T_{cycle}
T_{cycle}	Cycle that control center sends frequency regulation signals
$SC_{v,e}^P(k,t)$	Number of SCs that ESB e punctures remote user v in slot k of frame t
$SC_e^B(k,t)$	Number of SCs punctured by ESB e in slot k of frame t
$SC_e^B(\cdot)$	Number of SCs punctured by ESB e within a T_{cycle}
$SC_v^M(k,t)$	Number of SCs punctured from remote user v in slot k of frame t
$SC_v^*(t)$	Number of SCs that have been optimally allocated to remote user v in frame t
$I_{v,m}^*$	Optimized indicator of RBG allocation between remote user v and RBG m
U	Control parameter for the number of SCs that ESBs can puncture
$B_e^B(\cdot)$	Bandwidth punctured by ESB e within a T_{cycle}
D	Fixed size of frequency regulation signals transmitted from the BS to each ESB
O_e	Transmission order of ESB e
$SC_p(t)$	Total number of SCs available for ESBs to puncture in frame t .

I. INTRODUCTION

Grid frequency deviations can result in severe consequences, including equipment damage, system instability, and even large-scale blackouts. For example, on September 14, 2023, a line fire in Nigeria caused the system frequency to drop to 48.41 Hz, ultimately resulting in a total collapse of the power grid [1]. Similarly, on January 23, 2023, 220 million people in Pakistan were without power for nearly 22 hours due to chronic power frequency fluctuations in the south of the country [2]. These examples highlight the importance of frequency regulation for grid security.

Grid frequency deviations arise primarily from imbalances between supply and demand, typically caused by variations in load or generation. On the supply side, the increasing penetration of renewable energy sources like wind and photovoltaic presents significant challenges for frequency regulation in power grids due to their intermittent nature [3]. On the demand side, sudden changes in consumer usage or industrial load can cause deviations from the nominal frequency. Facing these challenges, existing frequency regulation mechanisms relying on traditional generation units cannot respond rapidly enough to frequency problems due to slower ramp rates and longer response times. Energy storage batteries (ESBs), as an ideal frequency regulation resource with fast ramp-up

times and flexible control capabilities, can offer an effective solution [4], [5]. The integration of ESBs helps maintain system power balance, ensuring frequency security despite the power fluctuations from supply and demand sides [6]–[8]. In practice, some provinces in China have launched energy storage-based frequency regulation projects [9], [10]. For example, on March 28, 2024, Jiangsu's first aggregated user-side distributed energy storage project was commissioned and connected to the grid in Nantong [9]. The project has a total capacity of 3,200 kW / 11,505 kWh and enables the aggregation of small-scale user-side storage systems to participate in unified grid frequency regulation. On July 2, 2025, in Yangjiang, Guangdong Province, the energy storage frequency regulation project at the Yangxi Power Plant passed final acceptance. This project is co-located with the largest single-unit coal-fired power plant in Asia and features a total installed and grid-connected capacity of 105 MW / 111.81 MWh [10].

Several studies investigate the impact of communication time delays on grid frequency regulation performance [11]–[13]. The authors in [11] investigate demand response scenarios where flexible loads adjust power consumption to provide frequency regulation services, and find that the communication delay of flexible loads impacts system frequency deviations. The impact of communication delays of energy storage facilities on the area control error is studied in [12], and the results show that the smaller the delay, the better the area control error. According to [13], the communication time delay will substantially impact the frequency regulation performance when the variable renewable energy penetration is above 40%. Based on the above literature, it is evident that when ESBs participate in grid frequency regulation to address sudden system frequency deviations, the communication time delay in receiving regulation signals is related to grid frequency regulation performance.

In practice, the control center usually sends frequency regulation signals to ESBs only after detecting a significant frequency deviation in the grid, and these signals continue until the frequency returns to normal. For such intermittent communication demands, wireless transmission is widely used because it offers great flexibility, rapid deployment, and cost efficiency [14], [15]. Nonetheless, wireless transmission faces the issue of limited spectrum resources [16], [17]. The above studies primarily focus on the relationship between communication time delay and grid frequency regulation performance, without delving into how the allocation of spectrum resources impacts grid frequency regulation performance. We consider a spectrum-limited scenario with two types of users where one class of wireless grid users requires continuous reception of large data volumes while ESBs need to intermittently receive smaller volumes of frequency regulation signals. On one hand, allocating fixed spectrum resources to ESBs with intermittent communication demands reduces the utilization efficiency of spectrum resources. On the other hand, if the spectrum resource is allocated to ESBs only when needed, the delay in transmitting the frequency regulation signal will become longer since the resource may not be available immediately. Therefore ESBs have to wait for other users to release the

spectrum.

The slice puncturing technique [18] is a promising solution to the above spectrum resource allocation issue, which dynamically reallocates subcarrier (SC) resources within a fifth-generation (5G) network to improve system flexibility and adaptability to varying traffic loads. Unlike static resource assignment, slice puncturing allows for real-time adjustments of SC allocations, optimizing network efficiency for applications with intermittent and high-priority communication needs. In recent years, the slice puncturing technique has achieved significant attention due to the growing demand for efficient resource allocation in wireless networks [19]–[21]. A model-free deep reinforcement learning (DRL)-based solution is proposed in [19] to minimize the throughput loss on enhanced mobile broadband (eMBB) terminals punctured by ultrareliable low latency communications (URLLC) terminals. The authors in [20] investigate a joint eMBB and URLLC scheduler, with the dual objectives of maximizing utility for eMBB traffic while immediately satisfying URLLC demands. The delay requirement of eMBB terminals under slice puncturing is considered in [21] and the simulation results show that the proposed method can satisfy both the delay requirement of eMBB terminals and the tight Quality-of-Service (QoS) requirement of URLLC terminals. The above studies focus on the coexistence of URLLC and eMBB users, aiming to design puncturing strategies to simultaneously meet the QoS requirements of both user types.

However, to the best of our knowledge, this is the first work to take the advantage of the slice puncturing technique to solve the challenge of grid frequency regulation. In our considered spectrum-limited scenario, ESBs puncture the spectrum resource of other grid users to receive frequency regulation signals when needed, thereby enhancing spectrum resource utilization while ensuring grid frequency regulation performance. In addition, when multiple ESBs participate in grid frequency regulation, the puncturing order of each ESB must be considered. This is because the puncturing order is related to the fair sharing of ESB, and failing to ensure the fair sharing can shorten ESB lifetimes. Therefore, the slice puncturing scheme for ESBs is worth further investigation. In this paper, we consider a spectrum-limited scenario where there are ESBs with intermittent transmission requirements and other grid users with continuous and substantial transmission demands. The main contributions of this article are as follows.

- We establish a grid frequency regulation structure that links frequency performance with spectrum resources and communication delay. This structure provides a modeling foundation for investigating spectrum resource allocation scheme, i.e., slice puncturing scheme, for ESBs to ensure grid frequency regulation performance.
- Due to the limited spectrum resources, we optimize the spectrum resource allocation of other grid users which will be punctured by ESBs when needed. Specifically, we formulate a spectrum resource optimization problem for these grid users. After that, to enhance computational efficiency, we transform and solve the optimization problem using virtual queues and a drift-plus-penalty function approach.

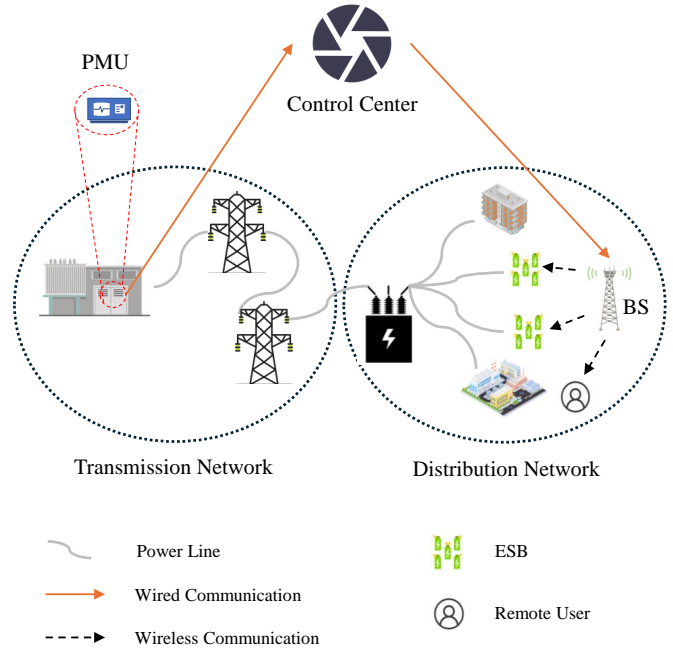


Fig. 1. A power-communication system model with two grid services: the remote service and the frequency regulation service.

- Considering limited spectrum resources, we develop a universal puncturing scheme for ESBs puncturing spectrum resources of other grid users. The scheme can significantly reduce the communication delay and improve the grid frequency regulation performance. In addition, our scheme can be implemented in a fair manner when multiple ESBs participate in the frequency regulation.

II. SYSTEM MODEL

A. Overview System Description

We consider a power-communication system with two types of services: the remote service and the frequency regulation service, as shown in Fig. 1. In such a power-communication system, the base station (BS) adopts 5G technologies to help the control center transmit data packets to two different types of users: remote users and ESBs. We use $\mathbb{V} = \{1, \dots, V\}$ and $\mathbb{E} = \{1, \dots, E\}$ to denote the set of remote users and ESBs, respectively.

This paper focuses on the downlink transmission. For the remote service, the control center transmits data packets to remote users over a period of time, and the transmit data size is relatively large but the transmission delay requirements are relatively low. On the other hand, for the frequency regulation service, the control center transmits small data packets to ESBs, but with higher delay requirements. Specifically, the control center will periodically monitor the system frequency. If the system frequency deviation exceeds a certain threshold, the control center will, with the assistance of the BS, send frequency regulation signals to ESBs. Upon receiving the signals, ESBs will immediately connect to the grid to assist in system frequency regulation. It is worth noting that, due to high delay requirements for the frequency regulation service, we also consider the time it takes for the Phasor Measurement

Unit (PMU) to detect and transmit the system frequency to the control center. Specifically, the total time delay of the frequency regulation signal to the ESB e can be expressed as

$$T_{\text{tl}}^e = T_{\text{PMU}} + T_c + T_b^e \quad \forall e \in \mathbb{E}, \quad (1)$$

where T_{PMU} denotes the time delay from the PMU to the control center; T_c and T_b^e denote the transmission delay from the control center to the BS and from the BS to the ESB e , respectively. Remarkably, we assume that T_{PMU} and T_c are fixed.

To sum up, the data packet size and transmission delay requirements differ between the remote service and the frequency regulation service. Therefore, it is worth investigating how the BS allocates spectrum resources to the remote service and the frequency regulation service.

B. Communication Model

Channel Model for Users: It is assumed that the BS has perfect knowledge of the channel state information (CSI) of the users (including remote users and ESBs) obtained from the pilot signal. The channel power gain for the i -th user can be expressed as

$$g_i = |h^i|^2 (d_i)^{-\varphi}, \quad (2)$$

where φ is the path-loss exponent; d_i is the distance from the BS to the i -th user. The small-scale fading h^i of the i -th user satisfies the distribution of $CN(0, 1)$ ($E[|h^i|^2] = 1$). Therefore, according to the Shannon formula, the data rate can be computed by

$$r_v^M = B_v^M \log_2 \left(1 + \frac{P_M g_v}{B_v^M N_0} \right) \quad \forall v \in \mathbb{V}, \quad (3)$$

$$r_e^B = B_e^B \log_2 \left(1 + \frac{P_B g_e}{B_e^B N_0} \right) \quad \forall e \in \mathbb{E}, \quad (4)$$

where P_M and P_B denote the transmit power of the BS to remote users and ESBs, respectively; B_v^M and B_e^B denote the allocated bandwidth to the v -th remote user and the e -th ESB, respectively; N_0 denotes the power spectral density of Gaussian white noise.

Dynamic Queue Model for the Remote Service: Let us consider a time-slotted system where t represents the t -th time slot. For the remote service, we adopt a dynamic queue model to formulate delay requirements. Specifically, the BS maintains data queues for each remote user $v \in \mathbb{V}$, and the queue backlog of each remote user can be represented as

$$Q_v(t+1) = \max \{Q_v(t) - R_v(t), 0\} + A_v(t) \quad \forall v \in \mathbb{V}, \quad (5)$$

where $A_v(t)$ is the arrival rate at the t -th time slot; $Q_v(t)$ is the queue backlog at the t -th time slot; $R_v(t)$ is the departure rate at the t -th time slot. For the arrival rate $A_v(t)$, we assume the traffic arrival of the remote user v follows the Poisson distribution with a mean of λ_v bits per time slot. In addition, the arrival rate $A_v(t)$ is independent over each time slot. For

the departure rate $R_v(t)$, we have $R_v(t) = r_v(t) \cdot T_s$, where T_s is the duration of one time slot.

Delay Requirement for the Remote Service: According to [21], the delay requirement of the remote service transformed from the queue backlog, is expressed as

$$\lim_{T \rightarrow \infty} \frac{1}{T} \sum_{t=0}^{T-1} Q_v(t) \leq \delta_v \quad \forall v \in \mathbb{V}, \quad (6)$$

where $\delta_v = \lambda_v l_v \omega$ denotes the threshold of the queue backlog of the v -th remote user; l_v denotes the delay requirement of the v -th remote user; ω denotes the maximum delay violation probability.

C. Frequency Response Model

We consider a system frequency response model of ESBs participating in system frequency regulation, as shown in Fig. 2. In the model, the reheat steam generator is used as an example of generation units, including the speed governor, the reheat steam turbine, and the generator. When the system power load ΔP_L suddenly changes, a system frequency deviation Δf is generated and can be detected by the PMU. The ESBs will output power, and the reheat steam generator will increase power generation to restore the system frequency to its rated value.

We can see from Fig. 2 that the power generation deviation ΔP_G is related to the speed governor model and the reheat steam turbine model. Hence, ΔP_G can be computed by

$$\begin{aligned} \Delta P_G &= \frac{1}{T_g s + 1} \times \frac{F_{\text{HP}} T_r s + 1}{(T_t s + 1)(T_r s + 1)} \times \left(-\frac{K}{s} - \frac{1}{R} \right) \times \Delta f \\ &= -\frac{(F_{\text{HP}} T_r s + 1)(K/s + 1/R)}{(T_g s + 1)(T_t s + 1)(T_r s + 1)} \Delta f, \end{aligned} \quad (7)$$

where T_g , T_t , and T_r denote the time constants of the speed governor, the turbine and the reheat process, respectively; F_{HP} denotes the high-pressure turbine's power fraction; K and R denote the proportional and integral gains, respectively. In addition, the total power output of energy storage batteries ΔP_B is the sum of the outputs of all E ESBs. Therefore, with ΔP_L , ΔP_G , and ΔP_B , the system frequency deviation Δf can be computed by

$$\Delta f = \frac{1}{2Hs + K_D} (\Delta P_G + \Delta P_B - \Delta P_L), \quad (8)$$

where H and K_D are the generator inertia and the load-damping factor, respectively.

III. SCHEDULING FOR THE REMOTE SERVICE

This section studies the efficient resource allocation to the remote users, and the allocated spectrum resources will be punctured by ESBs in Section IV.

A. Problem Formulation of Minimizing Spectrum Resources

As mentioned in Section II-B, the traffic arrival of the remote service follows the Poisson distribution per time slot, meaning that the amount of the remote service data needed to transmit differs per time slot. Thus, the spectrum resources

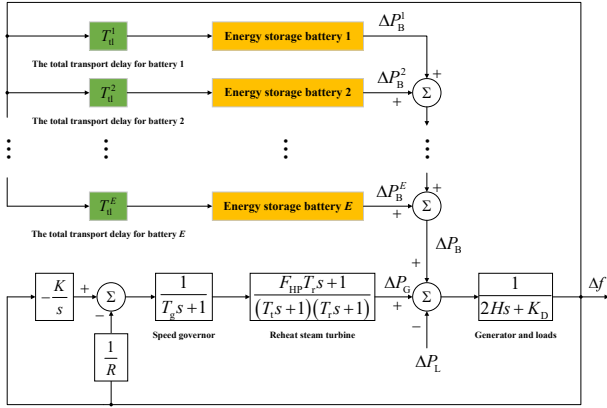


Fig. 2. A system frequency response model of ESBs participating in frequency regulation.

allocated to the remote service in each time slot should be scheduled rationally to minimize spectrum resource usage in a spectrum-limited scenario.

In this paper, 5G technologies are used on the downlink transmission from the BS to remote users. According to [22], 5G employs a flexible scheduling mechanism that can dynamically adjust time, and spectrum resources based on network demands. It supports various subcarrier spacings (15 kHz, 30 kHz, 60 kHz, 120 kHz, 240 kHz) and different frame structures, making resource allocation more adaptable. In 5G NR, a Resource Block is the most fundamental resource allocation unit in the time and frequency domains, typically comprising 12 subcarriers (in the frequency domain) and a set of OFDM symbols within a slot (in the time domain). Moreover, a Resource Block Group (RBG) is a collection of Resource Blocks. The scheduler can allocate resources based on RBGs rather than individual Resource Blocks, reducing signaling overhead and improving scheduling efficiency and flexibility. Therefore, considering the relatively low transmission delay requirement, the RBG is used in this paper as the resource allocation unit for the BS to transmit data packets to remote users.

Specifically, the RBG used in this paper comprises 12 subcarriers in the frequency domain and 10 milliseconds (ms) in the time domain. The bandwidth resource in a time slot (10 ms) is divided into a set of RBGs denoted by $\mathbb{M} = \{1, \dots, M\}$ and m denotes the index of the RBG. B_{sc} is used to denote the bandwidth of each SC. In each scheduling cycle (10 ms), the system allocates a certain number of RBGs to each remote user for the BS to transmit data. Specifically, if the m -th RBG is allocated to the v -th remote user at time slot t , the value of binary assignment variable $I_{v,m}(t)$ is 1; Otherwise, $I_{v,m}(t)$ equals 0.

We use Ω_1 to denote the total bandwidth resource usage for the remote users, that is, $\Omega_1 = \sum_{v \in \mathbb{V}} B_v(t) = \sum_{v \in \mathbb{V}} 12B_{sc} \sum_{m=1}^M I_{v,m}(t)$. Hence, the bandwidth allocation problem can be formulated as

$$\min_{I_{v,m}(t)} \Omega_1 \quad (9a)$$

$$\text{s.t. } I_{v,m}(t) = \{0, 1\} \quad \forall v \in \mathbb{V} \quad \forall m \in \mathbb{M} \quad (9b)$$

$$\sum_{v \in \mathbb{V}} I_{v,m}(t) \leq 1 \quad \forall m \in \mathbb{M} \quad (9c)$$

$$R_v(t) \leq Q_v(t) \quad \forall v \in \mathbb{V} \quad (9d)$$

$$\lim_{T \rightarrow \infty} \frac{1}{T} \sum_{t=0}^{T-1} Q_v(t) \leq \lambda_v l_v \omega \quad \forall v \in \mathbb{V} \quad (9e)$$

where the constraints (9b) and (9c) ensure that each RBG is allocated to one remote user at most. The constraint (9d) limits the departure rate for maximizing bandwidth resource utilization efficiency. Moreover, the constraint (9e) guarantees the statistical delay of remote users. It is worth noting that the constraint (9e) represents the long-term constraint for the queues backlog of remote users. Hence, the bandwidth allocation problem cannot be directly addressed using conventional optimization methods due to its long-term constraint. However, the Lyapunov optimization theory offers a framework to tackle such problems. Therefore, we transform the original bandwidth allocation problem into a series of short-term optimization problems in Section III-B.

B. Problem Transformation

To address the average queue backlog constraint (9e), we introduce the concept of virtual queues, transforming long-term constraints into a problem of virtual queue stability. We use $G_v(t)$ to define a virtual queue for each queue backlog. The update equation for each virtual queue is

$$G_v(t+1) = \max \{G_v(t) + Q_v(t+1) - \delta_v, 0\} \quad \forall v \in \mathbb{V}. \quad (10)$$

According to [21], the long-term constraint (9e) will be satisfied when the virtual queue $G_v(t)$ is stable ($\lim_{T \rightarrow \infty} (G_v(t)/T) = 0, \forall v \in \mathbb{V}$). Therefore, we reformulate each long-term constraint as a problem of ensuring the stability of purely virtual queues. That is, maintaining the long-term constraint is equivalent to ensuring the stability of the virtual queues. Consequently, the original bandwidth allocation problem can be transformed as follows:

$$\min_{I_{v,m}(t)} \Omega_1 \quad (11a)$$

$$\text{s.t. } I_{v,m}(t) = \{0, 1\} \quad \forall v \in \mathbb{V} \quad \forall m \in \mathbb{M} \quad (11b)$$

$$\sum_{v \in \mathbb{V}} I_{v,m}(t) \leq 1 \quad \forall m \in \mathbb{M} \quad (11c)$$

$$R_v(t) \leq Q_v(t) \quad \forall v \in \mathbb{V} \quad (11d)$$

$$\lim_{T \rightarrow \infty} \frac{G_v(t)}{T} = 0 \quad \forall v \in \mathbb{V} \quad (11e)$$

Subsequently, to address the issue of virtual queue stability (11e), we reformulate the above optimization problem into a series of short-term optimization problems using the drift-plus-penalty (DPP) method. Based on Lyapunov optimization

theory, for each time slot t , the weighted-Lyapunov function is constructed as follows

$$L(t) \triangleq \frac{V_1}{2} \sum_{v \in \mathbb{V}} G_v(t)^2, \quad (12)$$

where V_1 ($V_1 > 0$) is a control parameter for the virtual queues. The Lyapunov drift is defined as the change in the Lyapunov function (12) between two adjacent time slots, i.e.,

$$\Delta L(t) \triangleq L(t+1) - L(t). \quad (13)$$

According to the Lyapunov DPP method, we use the objective function Ω_1 as a penalty function. Then, the DPP function is computed by

$$\Delta L(t) + V_2 \Omega_1, \quad (14)$$

where V_2 ($V_2 > 0$) is the control parameter for the performance of the objective function. According to Lyapunov optimization theory, if the upper bound of the DPP function (14) exists, the virtual queue $G_v(t)$ is stable.

Next, we compute the upper bound of the DPP function (14). The Lyapunov drift between two adjacent time slots is

$$\Delta L(t) = L(t+1) - L(t) = \frac{V_1}{2} \sum_{v \in \mathbb{V}} (G_v(t+1)^2 - G_v(t)^2). \quad (15)$$

Since the constraint (9d) must be satisfied, the equation (5) can be updated by

$$Q_v(t+1) = Q_v(t) - R_v(t) + A_v(t) \quad \forall v \in \mathbb{V}. \quad (16)$$

Based on the virtual queue of queue backlog, we can derive

$$\begin{aligned} & G_v(t+1)^2 - G_v(t)^2 \\ &= \max \{G_v(t) + Q_v(t+1) - \delta_v, 0\}^2 - G_v(t)^2 \\ &\leq [G_v(t) + Q_v(t+1) - \delta_v]^2 - G_v(t)^2 \\ &= G_v(t)^2 + Q_v(t+1)^2 + \delta_v^2 + 2G_v(t)Q_v(t+1) \\ &\quad - 2G_v(t)\delta_v - 2Q_v(t+1)\delta_v - G_v(t)^2 \\ &\leq Q_v(t+1)^2 + \delta_v^2 + 2G_v(t)Q_v(t+1) \\ &= [Q_v(t) - R_v(t) + A_v(t)]^2 + \delta_v^2 \\ &\quad + 2G_v(t)[Q_v(t) - R_v(t) + A_v(t)] \\ &= Q_v(t)^2 + A_v(t)^2 + \delta_v^2 + 2Q_v(t)A_v(t) + R_v(t)^2 \\ &\quad + 2G_v(t)[Q_v(t) + A_v(t)] - 2R_v(t)[Q_v(t) + G_v(t)]. \end{aligned} \quad (17)$$

Hence, the upper bound of the DPP function is computed by

$$\begin{aligned} \Delta L(t) + V_2 \Omega_1 &= \frac{V_1}{2} \sum_{v \in \mathbb{V}} (G_v(t+1)^2 - G_v(t)^2) + V_2 \Omega_1 \\ &\leq \frac{V_1}{2} \sum_{v \in \mathbb{V}} (C_v + R_v(t)^2 - 2R_v(t)[Q_v(t) + G_v(t)]) + V_2 \Omega_1, \end{aligned} \quad (18)$$

where $C_v = Q_v(t)^2 + A_v(t)^2 + \delta_v^2 + 2Q_v(t)A_v(t) + 2G_v(t)[Q_v(t) + A_v(t)]$. The parameters V_1 and V_2 can be

adjusted to balance the trade-off between queue backlog and the utility function (bandwidth resource in this section). For instance, a large parameter V_2 implies that the bandwidth resource of remote users is given more priority.

Notably, since we can know all previous states (including δ_v , $A_v(t)$, $Q_v(t)$ and $G_v(t)$), at any time slot t , $\sum_{v \in \mathbb{V}} C_v$ can be regarded as a fixed parameter for each time slot. Hence, the upper bound of the DPP function can be updated by $\Omega_2 = \frac{V_1}{2} \sum_{v \in \mathbb{V}} [R_v(t)^2 - 2R_v(t)[Q_v(t) + G_v(t)]] + V_2 \Omega_1$.

Based on the Lyapunov optimization framework, the upper bound of the DPP function Ω_2 can be substituted as the objective function for the short-term optimization problem. Moreover, the constraint (11e) can be satisfied if Ω_2 is minimized. Thus, the short-term optimization problem is shown as follows:

$$\min_{I_{v,m}(t)} \Omega_2 \quad (19a)$$

$$\text{s.t. } I_{v,m}(t) = \{0, 1\} \quad \forall v \in \mathbb{V} \quad \forall m \in \mathbb{M} \quad (19b)$$

$$\sum_{v \in \mathbb{V}} I_{v,m}(t) \leq 1 \quad \forall m \in \mathbb{M} \quad (19c)$$

$$R_v(t) \leq Q_v(t) \quad \forall v \in \mathbb{V} \quad (19d)$$

The short-term optimization problem is a 0-1 integer programming problem with the set of variable $I_{v,m}(t) = \{0, 1\}$, $\forall v \in \mathbb{V}, \forall m \in \mathbb{M}$.

C. Solution of Minimizing Spectrum Resources

According to the matching theory, we transfer the short-term optimization problem into a series of one-to-one matching problems. Specifically, we allocate each RBG to a potential remote user step by step until one of these three cases happens:

- (1) All the M RBGs have been allocated.
- (2) The constraint (19d) can not be met for any remote user.
- (3) The value of Ω_2 does not decline.

In the one-to-one matching problem, all remote users will compete for one RBG. However, only the remote user benefiting the objective function Ω_2 most can successfully obtain the RBG. Assuming the v -th remote user has obtained η_v RBGs, then a metric denoted by $D_v(t)$ is used to measure the degree of demand of the users for another RBG, which is computed by

$$\begin{aligned} D_v(t) &= \hat{R}_v(t)^2 - \check{R}_v(t)^2 \\ &\quad - 2[Q_v(t) + G_v(t)](\hat{R}_v(t) - \check{R}_v(t)) \quad \forall v \in \mathbb{V}, \end{aligned} \quad (20)$$

where $\hat{R}_v(t)$ and $\check{R}_v(t)$ denote the departure rates when the number of allocated RBGs are $\eta_v + 1$ and η_v , respectively. Moreover, the smaller the value of $D_v(t)$ is, the more the user wants the RBG. Hence, the optimal remote user will be selected according to the following expression:

$$v^* = \arg \min_v D_v(t) \quad \forall v \in \mathbb{V}. \quad (21)$$

TABLE I
STRATEGY OF SOLVING THE SHORT-TERM OPTIMIZATION PROBLEM

Algorithm 1: OTOM

```

1: Initialize binary assignment variable  $I$  and let  $m = 1, \forall v \in \mathbb{V}, \eta_v = 0$  ;
2: while  $m \leq M$ :
3:   Update  $\hat{R}_v(t)$  and  $\check{R}_v(t)$  ;
4:   Select the optimal remote user  $v^*$  for the  $m$ -th RBG
5:   based on (21) and restricted by (19d);
6:   if the value of  $\Omega_2$  does not decline:
7:     break;
8:   end if
9:   Update  $m$ , and  $\eta_{v^*} = \eta_{v^*} + 1$ ;
10: end while
11: Get the optimal  $I^*$ .

```

After selecting the optimal remote user v^* for the m -th RBG, the number of allocated RBGs needs to be updated. The system then continues to solve the one-to-one matching problem for another RBG based on equation (21). Consequently, we simplify the 0-1 integer programming problem into a series of matching issues which can be easily solved. Based on the above analysis, the one-to-one matching (OTOM) algorithm for solving the short-term optimization problem is summarized in Table I.

IV. SCHEDULING FOR FREQUENCY REGULATION SERVICE

This section presents a slice puncturing scheme for ESBs to lower the transmission delay for better grid frequency performance.

A. The Relationship between the Time Delay and the Frequency Regulation Performance

To investigate the seriousness of time delay in the frequency regulation scenario, the relationship between the time delay and the frequency performance can be given as Fig. 2. Specifically, we consider a steam turbine generator with a generation capacity of 800 MW. The time constants of the speed governor (T_g), the turbine (T_t), and the reheating process (T_r) are set to 0.2 s, 0.3 s, and 7 s, respectively. In addition, The high-pressure turbine's power fraction (F_{HP}), the speed droop parameter (R), and the integral gain (K) are 0.3, 0.05, and 0.5, respectively. The generator inertia (H) is set to 10, and the load-damping factor (K_D) is set to 1. The rated frequency of the power system is 50 Hz. The total simulation duration is 400 s, during which the system power load ΔP_L changes from 70% to 80% at 300 s. In practical applications, the ramp rate constraint of the generator must be considered, which is set as 3% per minute. After a steam turbine unit is connected to the grid and operating stably, there is a limit ($\pm 6\%$ in this paper) to the change in its output power during frequency regulation. T_{cycle} is used to denote the cycle that the control center sends the frequency regulation signals ($T_{cycle} = 0.1$ s in this section).

We use $P_{rp} = \{P_{rp}^1, \dots, P_{rp}^E\}$ to denote the set of rated powers of ESBs. Specifically, a total of 10 ESBs, where ESB 1 to 5 have a rated power of 6 MW ($P_{rp}^1 = \dots = P_{rp}^5 = 6\text{MW}$), and ESB 6 to 10 have a rated power of 10 MW ($P_{rp}^6 = \dots = P_{rp}^{10} = 10\text{MW}$), are considered in this section. Furthermore, we established the following regulations

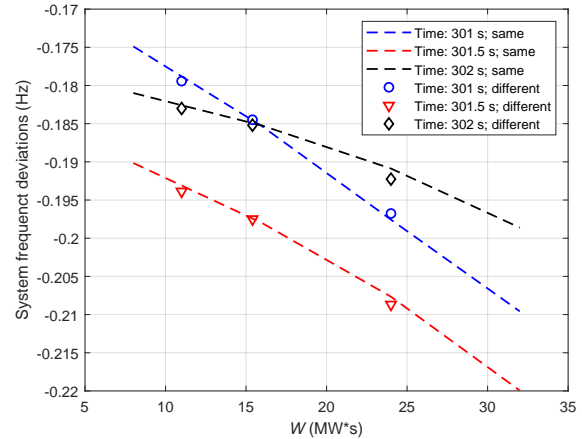


Fig. 3. The frequency deviations of the grid versus W when the system time is 301 s, 301.5 s, and 302 s.

for battery participation in frequency regulation: when the system frequency deviation first reaches -0.02 Hz, ESB 1 through 5 will output power; when the system frequency deviation first reaches -0.1 Hz, all ESBs will participate in frequency regulation.

As shown in Table II, we consider seven schemes with different kinds of total time delay, where $W = \sum_{i=1}^{10} T_{tl}^i P_{rp}^i$ is the sum of the products of each ESB's total time delay and its rated power. Specifically, the total time delays to the 10 ESBs are the same among the front four schemes and differ among the rest three schemes. Based on Table II, Fig. 3 plots the frequency deviations of the power system versus W when the system time is 301 s, 301.5 s, and 302 s. As shown in Fig. 3, regardless of whether the total time delay of each ESB is the same, the system frequency deviation exhibits an approximately linear relationship with W when the system time is fixed. In addition, the smaller the value of W , the smaller the system frequency deviation. Furthermore, as discussed in Section II-A, $T_{tl}^e = T_{PMU} + T_c + T_b^e$ (T_{PMU} and T_c are both fixed). Hence, the smaller $\sum_{e \in \mathbb{E}} T_b^e P_{rp}^e$ is, the smaller system frequency fluctuations are. To optimize the system frequency performance, we should reduce the transmission delay from the BS to ESBs T_b^e as much as possible.

However, in the practical grid, the system power load ΔP_L often changes suddenly, so reserving fixed RBG for the frequency regulation service results in the wastage of bandwidth resources. On the other hand, when frequency regulation traffic arrives suddenly, temporary allocation of additional RBGs typically introduces significant control latency, largely improving the end-to-end time delay. Therefore, we introduce the slice puncturing technique in 5G to reduce transmission delay from the BS to ESBs in the next subsection.

B. Slice Puncturing Problem Formulation

According to NR Release-15 [23], a frame has a duration of 10 ms and contains 10 subframes, each with a duration of 1 ms. The number of slots per subframe depends on the subcarrier spacing, ranging from 1 slot (subcarrier spacing of 15 kHz) to 16 slots (subcarrier spacing of 240 kHz). In this paper, we only consider the case with a subcarrier spacing of

TABLE II
THE DIFFERENT SCHEMES WITH SEVERAL KINDS OF END-TO-END TIME DELAY

Scheme	T_{tl}^1 (s)	T_{tl}^2 (s)	T_{tl}^3 (s)	T_{tl}^4 (s)	T_{tl}^5 (s)	T_{tl}^6 (s)	T_{tl}^7 (s)	T_{tl}^8 (s)	T_{tl}^9 (s)	T_{tl}^{10} (s)	W (MW*s)
1	0.1	0.1	0.1	0.1	0.1	0.1	0.1	0.1	0.1	0.1	8
2	0.2	0.2	0.2	0.2	0.2	0.2	0.2	0.2	0.2	0.2	16
3	0.3	0.3	0.3	0.3	0.3	0.3	0.3	0.3	0.3	0.3	24
4	0.4	0.4	0.4	0.4	0.4	0.4	0.4	0.4	0.4	0.4	32
5	0.1	0.2	0.3	0.4	0.5	0.5	0.4	0.3	0.2	0.1	24
6	0.2	0.2	0.2	0.2	0.2	0.1	0.1	0.1	0.1	0.1	11
7	0.1	0.2	0.3	0.1	0.2	0.3	0.1	0.2	0.3	0.1	15.4

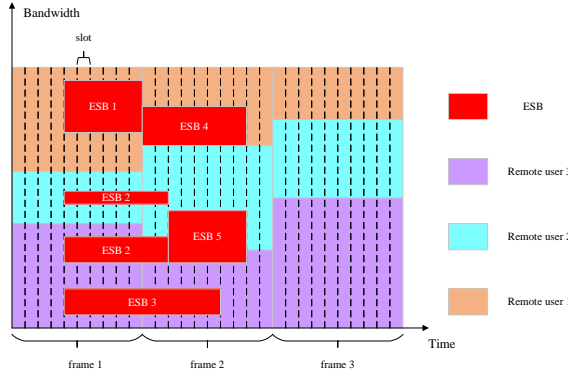


Fig. 4. An example of the process of ESBs puncturing remote users.

15 kHz, where each subframe contains one slot. As in Section III, the duration of one slot occupies 10 ms, which is equivalent to a frame of 5G. Henceforth, we will use 'frame' to refer to a time slot in Section II-B, and the slot duration will be 1 ms rather than 10 ms. We use k to denote the index of the slot in each frame, and $k \in \mathbb{S}, \mathbb{S} = \{1, \dots, 10\}$.

As discussed in Section IV-A, the frequency regulation packet will be transmitted every T_{cycle} only when the control center finds out that the system frequency deviation first reaches -0.02 Hz. We set that the arriving frequency regulation packet to BS is scheduled immediately to transmit in the next slot on top of the ongoing remote service transmissions. In other words, we control the queuing delay of ESBs within a slot duration.

Fig. 4 plots an example of the process of ESBs puncturing remote users. To describe the puncturing situation in a slot, we define a puncturing variable denoted by $SC_{v,e}^p(k, t)$ which represents the number of SCs that the e -th ESB punctures the v -th remote user in slot k of frame t . Moreover, each ESB may puncture more than one remote user to obtain enough SCs for transmission. Hence, the number of SCs punctured by the e -th ESB in slot k of frame t is calculated by

$$SC_e^B(k, t) = \sum_{v \in \mathbb{V}} SC_{v,e}^p(k, t) \quad \forall e \in \mathbb{E} \quad \forall k \in \mathbb{S}. \quad (22)$$

For example, as shown in Fig. 4, the number of SCs punctured by ESB 2 in slot 5 of frame 1 can be expressed as $SC_2^B(5, 1) = SC_{2,2}^p(5, 1) + SC_{3,2}^p(5, 1)$. Furthermore, we set the number of SCs punctured by each ESB to remain constant across different slots. Since each ESB will puncture the SCs of users at most once during each T_{cycle} , we use $SC_e^B(\cdot)$ to denote the number of SCs punctured by the e -th ESB within T_{cycle} . For example,

as shown in Fig. 4, the number of SCs punctured by ESB 3 is equal from the 5-th slot of frame 1 to the 6-th slot of frame 2, that is, $SC_3^B(5, 1) = SC_3^B(6, 1) = \dots = SC_3^B(6, 2) \triangleq SC_3^B(\cdot)$.

On the other hand, the SCs of each remote user within a frame may be punctured by more than one ESB. Therefore, the number of SCs punctured from the v -th remote user in slot k of frame t is calculated by

$$SC_v^M(k, t) = \sum_{e \in \mathbb{E}} SC_{v,e}^p(k, t) \quad \forall v \in \mathbb{V} \quad \forall k \in \mathbb{S}. \quad (23)$$

As shown in Fig. 4, the number of SCs punctured from remote user 3 in slot 5 of frame 1 can be expressed as $SC_3^M(5, 1) = SC_{3,2}^p(5, 1) + SC_{3,3}^p(5, 1)$.

As discussed in Section III, the allocated RBGs for each remote user remain constant within a frame. Hence, the number of SCs that have been optimally allocated to the v -th remote user in frame t is denoted by

$$SC_v^*(t) = 12 \sum_{m=1}^M I_{v,m}^*(t) \quad \forall v \in \mathbb{V}, \quad (24)$$

where $I_{v,m}^*(t)$ is optimized based on the scheme in Section III. To ensure that the number of SCs lost due to puncturing for each remote user remains within a controllable range, we impose the following constraints:

$$SC_v^M(k, t) \leq U \cdot SC_v^*(t) \quad \forall v \in \mathbb{V} \quad \forall k \in \mathbb{S}, \quad (25)$$

where U ($0 < U < 1/2$) is the control parameter for the number of SCs that ESB can puncture.

The bandwidth punctured by the e -th ESB can be computed by $B_e^B(\cdot) = B_{sc} \times SC_e^B(\cdot)$, where B_{sc} is the bandwidth of each subcarrier. Based on (4), the data rate for the e -th ESB is computed by

$$r_e^B(\cdot) = B_e^B(\cdot) \log_2 \left(1 + \frac{P_B g_e}{B_e^B(\cdot) N_0} \right). \quad (26)$$

We use D and O_e to denote the fixed data size of the frequency regulation signal transmitted from BS to ESBs and the transmission order of the e -th ESB, respectively. According to the formula (26), the more SCs an ESB acquires through puncturing, the faster the BS transmits the frequency regulation signal to that ESB. However, in this paper, a higher transmission rate does not necessarily imply a lower transmission delay due to the different transmission orders. For example, as shown in Fig. 4, ESB 5 punctures more SCs than ESB 2 ($SC_5^B(\cdot) > SC_2^B(\cdot)$), while the transmission delay from the BS to ESB 5 ($T_b^5 = T_b^2 + \lceil D/r_5^B(\cdot) \rceil$) is larger

than it from the BS to ESB 2 ($T_b^2 = \lceil D/r_2^B(\cdot) \rceil$). That is because the transmission order of ESB 2 precedes that of ESB 5 ($O_2 < O_5$). Hence, the transmission delay from the BS to the e -th ESB T_b^e can be divided into two parts: the sending time t_b^e and the queuing time t_q^e . Specifically, t_b^e is related to the number of SCs punctured by the ESB $SC_e^B(\cdot)$, and t_q^e is in connection with the transmission order O_e .

Furthermore, the control center sends the frequency regulation signals every T_{cycle} , and we have

$$T_b^e \leq T_{\text{cycle}} - T_{\text{PMU}} - T_c \quad \forall e \in \mathbb{E}. \quad (27)$$

As discussed in Section IV-A, the system frequency performance is related with $\sum_{e \in \mathbb{E}} T_b^e P_{\text{rp}}^e$. Therefore, we can optimize the system frequency performance by formulating the following minimization problem:

$$\min_{SC_{v,e}^P(k)} \sum_{e \in \mathbb{E}} T_b^e P_{\text{rp}}^e \quad (28a)$$

$$\text{s.t. } SC_v^M(k,t) \leq U \cdot SC_v^*(t) \quad \forall v \in \mathbb{V} \quad \forall k \in \mathbb{S} \quad (28b)$$

$$T_b^e \leq T_{\text{cycle}} - T_{\text{PMU}} - T_c \quad \forall e \in \mathbb{E} \quad (28c)$$

However, there is a practical contradiction in the above optimization problem. In the practical process of frequency regulation involving ESBs, the load should be distributed evenly among multiple ESBs to extend their lifespan. On the other hand, due to the varying rated power of each ESB, the BS will consistently allocate more bandwidth resources and more preferential transmission orders to those with higher rated power to minimize the optimization objective $\sum_{e \in \mathbb{E}} T_b^e P_{\text{rp}}^e$.

In other words, the ESBs with higher rated power will participate in frequency regulation for a longer duration and provide greater output, thereby affecting their performance and longevity. Therefore, rather than solve the optimization problem, we design a universal slicing puncturing (USP) scheme in the next subsection.

C. Universal Slice Puncturing Scheme

The puncturing scheme, including the number of SCs punctured and the transmission order for each ESB, is related to the total number of SCs available for ESBs to puncture in frame t , which can be computed by

$$SC_p(t) = U \cdot \sum_{v=1}^V SC_v^*(t). \quad (29)$$

The number of available SCs includes the following two cases:

- **Case A:** the available SCs are sufficiently large for all ESBs to puncture simultaneously. In this case, each ESB can immediately puncture SCs for data transmission, that is, $O_e = 1, \forall e \in \mathbb{E}$.
- **Case B:** the available SCs are insufficient for all ESBs to puncture simultaneously. In this case, some ESBs will puncture first while others will puncture later, that is, $\exists e \in \mathbb{E}, O_e = 2$.

The two different cases also introduce corresponding challenges in the following:

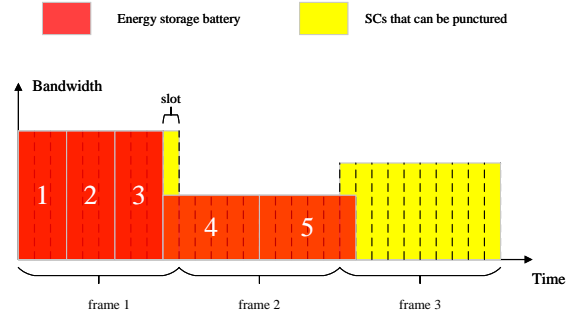


Fig. 5. An example of the designed universal slice puncturing scheme.

- **Challenges in case A:** if the available SCs cannot be evenly distributed among ESBs, it becomes necessary to determine which ESB should receive more SCs and how many additional SCs should be allocated.
- **Challenges in case B:** when the transmission orders among ESBs are different, it is essential to consider how many transmission orders exist and which ESBs are involved in each order. Additionally, when several ESBs puncture SCs within the same transmission order, the challenge of how to allocate excess SCs observed in case A will also arise in case B.

As discussed in Section III, the total number of SCs available for ESBs to puncture may vary across different frames due to the fluctuating number of SCs allocated to each remote user in each frame. On the other hand, the control center's cycle T_{cycle} for sending frequency regulation signals undoubtedly spans several frames (the duration of each frame is 10 ms). Hence, within a frequency monitoring cycle T_{cycle} , the available SCs could either fall under case A or case B. That is to say, we may encounter challenges from both case A and case B simultaneously within a T_{cycle} .

To overcome the above challenges, we design a USP scheme that is applicable regardless of SC_p . Fig. 5 plots an example of the designed USP scheme. Firstly, to address the challenge of allocating the potential excess SCs, our approach employs a single ESB to occupy all available SCs. As shown in Fig. 5, all available SCs for puncturing are allocated to ESB 1, and after ESB 1 receives the data, the SCs are then allocated to ESB 2. After that, to address the challenge of determining which ESB punctures first, our approach assigns a random transmission order to each ESB. Specifically, in each T_{cycle} , all ESBs participating in frequency regulation are randomly assigned a puncturing order with equal probability. Notably, the design of randomly assigning the puncturing order addresses the fair sharing issue, which could not be resolved by the optimization scheme presented in Section IV-B.

Moreover, the transmission time from the BS to an ESB may span across different frames, e.g., ESB 4 shown in Fig. 5. Given that SC_p of different frames may be different, we adopt the strategy that the number of SCs punctured by the ESB is the smallest among the frames involved. For example, as shown in Fig. 5, the number of SCs punctured by ESB 4 equals the available SCs in frame 2 because $SC_p(2) < SC_p(1)$. Similarly, since $SC_p(2) < SC_p(3)$, the number of SCs punctured by ESB 5 is consistent with the number provided

TABLE III
STRATEGY OF SOLVING THE SLICE PUNCTURING PROBLEM

Algorithm 2: USP

```

1: Initialize  $E$ ,  $SC_p$  and let  $e = 1$ ,  $t = 1$ ,  $t_s = 0$ ;
2: while  $e \leq E$ :
3:   Allocate  $SC_p(t)$  SCs to the  $e$ -th ESB and calculate  $t_b^e$ ;
4:   if  $t_s$  and  $t_s + t_b^e$  span across different frames:
5:     if  $SC_p(t) > SC_p(t+1)$ :
6:       Reallocate  $SC_p(t+1)$  SCs to the  $e$ -th ESB and recalculate  $t_b^e$ ;
7:     end if
8:   end if
9:   Update  $t$  based on  $t_s$  and  $t_s + t_b^e$ , and  $t_s = t_s + t_b^e$ ,  $e = e + 1$ ;
10: end while
11: Assign the puncturing order  $O_e$  randomly for each ESB;
12: Get the transmission delay  $T_b^e$  for each ESB within a  $T_{cycle}$ .

```

in frame 2. We use t_s to denote the sum of t_b^e within a T_{cycle} . The proposed algorithm is given in Table III in detail.

According to Table III, we can compute the transmission delay T_b^e for each ESB within a T_{cycle} with the algorithmic time complexity of $O(E)$.

V. PERFORMANCE EVALUATION

This section investigates the grid frequency regulation performance using slice puncturing technology. We first introduce the test settings including the value of related parameters, and some details of the test model. After that, we examine the grid frequency regulation performance of our proposed USP scheme.

A. Test Settings

In our test, we suppose that there is 1 remote user ($\mathbb{V} = \{1\}$) and 10 ESBs ($\mathbb{E} = \{1, \dots, 10\}$). The parameter settings for 10 ESBs are shown in Table IV. The path-loss exponent φ is set to 4, and the transmit power of the BS to the remote user (P_M) and ESBs (P_B) are both set to 0.5 W. In addition, the delay requirement l_1 and the maximum delay violation probability ω_1 are set to 0.5 s and 0.0001, respectively. The remote user's arrival rate A_1 follows the Poisson distribution with a mean of $\lambda_1 = 20$ kbits/0.01s within 400 s. The total number of RBGs is 4 ($\mathbb{M} = \{1, \dots, 4\}$). The control parameters V_1 and V_2 are both set to 1. Furthermore, the control parameter for the number of available SCs U is set to 5/12. The values of T_{PMU} and T_c are both set to 20 ms. The size of the frequency regulation signal D transmitted from the BS to each ESB is set to 1600 bits. The frequency regulation signals sending cycle T_{cycle} is 0.1 s, and other settings about the power system are the same as those in Section IV-A. Furthermore, we define the duration from receiving frequency regulation signals to power output delivery as the response time. The ESBs considered in this paper are lithium batteries. In the case analysis of this section, the response time of the ESB is set to be 0 s. On the other hand, the response time of the steam turbine is set to be 2 s.

Based on the above settings, we simulate the system frequency response model shown in Fig. 2 to investigate the frequency regulation performance under the USP scheme. Firstly, we initialize all parameters and then obtain the optimal RBG allocation scheme I^* within 400 s based on the OTOM algorithm mentioned in Table I. According to the formula (24)

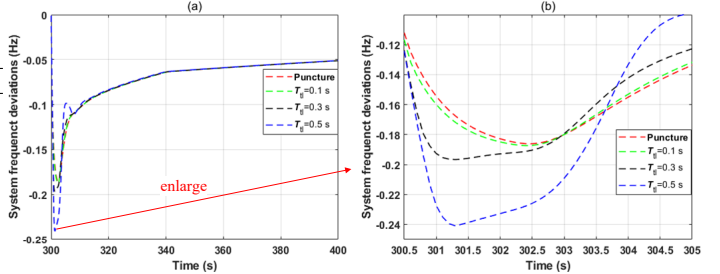


Fig. 6. Performance comparison with/without using the slice puncturing technology: the frequency deviations of the grid versus the system time T , (a) original figure in $T \in [300, 400]$, and (b) enlarge figure in $T \in [300.5, 305]$.

and (29), we can get the available SCs within 400 s, which serves as an initial input for our system frequency response model. In our test model, each ESB will experience a delay T_{tl}^e in receiving Δf , which depends on its transmission order and the number of allocated SCs. On the other hand, after receiving the current cycle's Δf with different delays, each ESB adjusts its output accordingly. For example, as shown in Table IV, if $0.02 \text{ Hz} < |\Delta f| \leq 0.04 \text{ Hz}$ for the first time, only ESB 1 and 2 will output power.

In the next subsection, the frequency regulation performance of the USP scheme will be analyzed numerically.

B. Frequency Regulation Performance Verification with Developed Puncturing Scheme

1) *Performance comparison with/without using the slice puncturing technology:* We investigate the grid frequency regulation performance of the proposed USP scheme after 300 s considering that the system power load ΔP_L changes from 70% to 80% at 300 s. Moreover, there are no fixed RBGs allocated for ESBs when the slice puncturing technology is not used. Hence, the time delay from the BS to ESBs is difficult to determine due to the queuing delay caused by waiting for the remote user to pause its transmission. In this section, the total time delay from when the control center starts to detect the system frequency to when ESBs receive the signal is assumed to be 0.1 s, 0.3 s, and 0.5 s for simplicity.

Fig. 6 plots the grid frequency deviations with/without using the slice puncturing technology under the different ranges of system time T . It can be seen from Fig. 6(a) that the frequency deviations first decrease to the maximum frequency deviation (MFD), and then exhibit an increasing trend.

As shown in Fig. 6(b), the MFD of the puncturing scheme is -0.1861. On the other hand, the MFD is -0.1874, -0.1967, and -0.241 when the total time delay is 0.1 s, 0.3 s, and 0.5 s. Specifically, the MFD of our proposed USP scheme can increase from -0.241 to -0.1861 by 22.8% compared with the case where the total time delay is 0.5 s.

2) *Performance comparison with different T_{cycle} :* Fig. 7 plots the grid frequency deviations when the frequency regulation signals sending cycle T_{cycle} is different. It can be seen from Fig. 7 that the frequency regulation performance decreases as T_{cycle} increases from 0.1 s to 0.3 s. For example, as shown in Fig. 7, the MFD is -0.1967, -0.2077, -0.2195 when T_{cycle} is 0.1 s, 0.2 s, 0.3 s and the total time delay T_{tl}

TABLE IV
PARAMETER SETTINGS FOR 10 ESBs

ESB No.	1	2	3	4	5	6	7	8	9	10
Rated power (MW)	4	4	6	6	8	8	10	10	12	12
Capacity (MWh)	2	4	3	6	4	8	5	10	6	12
Initial SoC	0.62	0.41	0.73	0.55	0.34	0.68	0.47	0.59	0.52	0.38
Distance to BS (m)	842	1123	765	1340	987	908	1562	679	1205	1031
Output threshold (Hz)	0.02	0.02	0.04	0.04	0.06	0.06	0.08	0.08	0.1	0.1

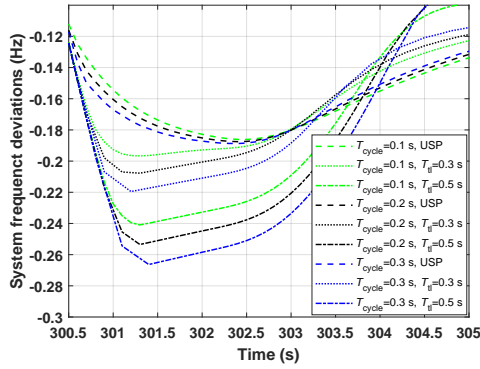


Fig. 7. Performance comparison with different T_{cycle} (the cycle that control center sends the frequency regulation signals): the frequency deviations of the grid versus the system time T .

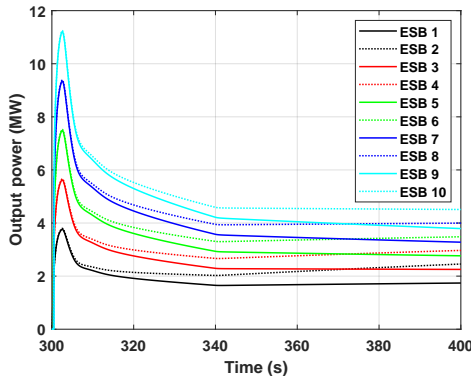


Fig. 8. Performance comparison with 10 ESBs: the output power versus the system time T .

is 0.3 s. Furthermore, our proposed USP scheme demonstrates greater advantages as T_{cycle} increases. For example, comparing the USP scheme and the case $T_{tl} = 0.5$ s, the MFD increases from -0.2663 to -0.1887 by 29.1% when $T_{cycle} = 0.3$ s, which is larger than 22.8% when $T_{cycle} = 0.1$ s.

3) *Operational status analysis for the ESB*: As shown in Table IV, we set the total rated power of the ESBs to match the magnitude of the introduced disturbance, i.e., 80 MW. Upon receiving the frequency regulation signal, each ESB immediately determines its output based on a PID control strategy, with the response time set to zero. On the other hand, following the disturbance, the steam turbine exhibits a 2-second response time.

Fig. 8 plots the different output powers of 10 ESBs from 300 s to 400 s. As illustrated in Fig. 8, the output powers of ESBs rapidly increase within the first several seconds, and then gradually decrease. This behavior arises because the ESBs must rapidly supply power to maintain frequency

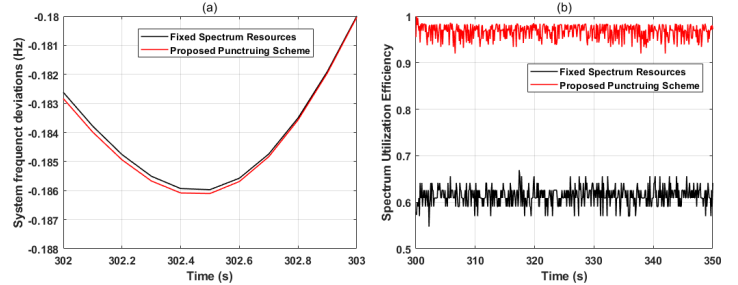


Fig. 9. Performance comparison between the fixed spectrum scheme and the puncturing scheme: (a) the frequency deviations of the grid, and (b) spectrum utilization efficiency versus the system time T .

balance in the period before the steam turbine contributes to frequency regulation. Once the turbine begins to contribute, the ESBs reduce their output accordingly. On the other hand, the overlapping output of ESBs with identical rated power during the rising phase is due to the use of the same output threshold and proportional gain settings. Furthermore, it can be seen from Fig. 8 that during the descending phase of the output, ESBs with smaller energy capacity deliver less power under the same rated power setting. This is due to the assignment of smaller integral gains to lower-capacity ESBs under equal rated power conditions.

4) *Quantitative analysis for spectrum utilization efficiency*: We consider an alternative scheme where an additional fixed RBG is allocated exclusively for frequency regulation service, serving as a benchmark for comparison against our proposed puncturing-based scheme in terms of spectrum utilization efficiency. Here, spectrum utilization efficiency is defined as the ratio of utilized subcarriers over allocated subcarriers within a given time window, rather than conventional spectral efficiency measured in bits/Hz.

Fig. 9 plots the performance comparison between the fixed spectrum scheme and the puncturing scheme on the frequency deviations of the grid, and spectrum utilization efficiency. Specifically, spectrum utilization efficiency is calculated every 0.1 s. As shown in Fig. 9(a), the fixed spectrum scheme only increases the MFD from -0.1861 to -0.1860 compared with our proposed puncturing scheme. On the other hand, the fixed spectrum scheme decreases spectrum utilization efficiency from over 0.9 to nearly 0.6, as shown in Fig. 9(b). Hence, the proposed puncturing scheme can achieve higher spectrum utilization efficiency while ensuring the QoS of the frequency regulation service compared with the fixed spectrum scheme.

5) *Performance comparison of systems of different scales*: We compare the frequency performance of three power systems with respective capacities of 160 MW, 800 MW, and 1600 MW. Specifically, the magnitude of disturbance introduced in

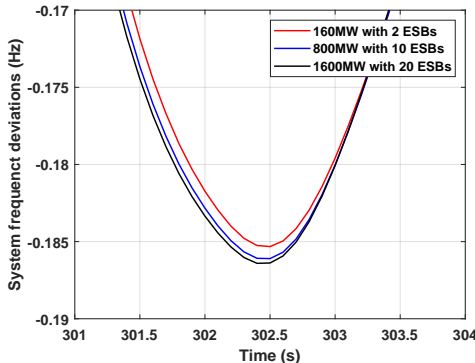


Fig. 10. Performance comparison among systems of different scales: the frequency deviations of the grid versus the system time T .

each system is set to 10% of its capacity, corresponding to 16 MW, 80 MW, and 160 MW, respectively. The total capacity of ESB participating in frequency regulation is configured to match each system's disturbance magnitude. The ESB configurations are as follows:

- 60 MW system with 2 ESBs (rated powers: 6 MW, 10 MW).
- 800 MW system with 10 ESBs (rated powers: 4 MW, 4 MW, 6 MW, 6 MW, 8 MW, 8 MW, 10 MW, 10 MW, 12 MW, 12 MW).
- 1600 MW system with 20 ESBs (rated powers: 4 MW \times 4, 6 MW \times 4, 8 MW \times 4, 10 MW \times 4, 12 MW \times 4).

Fig. 10 plots performance comparison when the system scale is 160 MW, 800 MW, and 1600 MW. As shown in Fig. 10, the MFD is -0.1853, -0.1861, and -0.1864 when the number of ESB is 2, 10, and 20. As the number of ESBs increases, the system frequency performance exhibits a slight decreasing trend. Therefore, under the premise of identical disturbance-to-system-capacity ratios and fixed ESB specifications, the quantity of ESB demonstrates a negligible impact on frequency performance when employing our puncture scheme.

6) Performance comparison of different types of equipment (ESBs and other frequency regulation systems): We consider configuring the response time of ESBs to 0.5 and 1 seconds to simulate other frequency regulation resources. Fig. 11 plots the performance comparison among different types of equipment when the system scale is 160 MW. As illustrated in Fig. 11, the MFD is -0.1853, -0.2461, and -0.3617 when the response time is 0 s (ESB), 0.5 s, and 1 s. Obviously, as the response time increases, the MFD gradually decreases. Moreover, when the response time reaches 1 s, the output lag of the frequency regulation resource is large, which leads to continuous frequency fluctuations.

To sum up, the proposed USP scheme can reduce the total time delay of ESBs receiving frequency regulation signals, improving the grid frequency regulation performance in terms of MFD.

VI. CONCLUSION

In this paper, we design a slice puncturing scheme to address the spectrum allocation issue between ESBs and other grid users in a spectrum-limited scenario. Performance evaluation

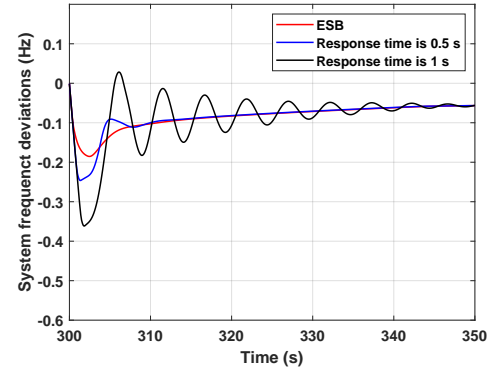


Fig. 11. Performance comparison among different types of equipment when the system scale is 160 MW: the frequency deviations of the grid versus the system time T .

demonstrates that our proposed puncturing scheme enhances spectrum utilization efficiency while ensuring the QoS of the frequency regulation service. Our approach provides insights into how to allocate spectrum resources to grid users in scenarios where spectrum is highly scarce, such as post-disaster communication reconstruction. Currently, we have focused on a simple communication scenario involving a single base station. Future work will also explore more complex scenarios, where multiple base stations can transmit signals to the same ESB.

REFERENCES

- [1] Izuaka M, Why national grid collapsed – Minister; 2023. [online]. Available: <https://www.premiumtimesng.com/news>.
- [2] S. Saifi, A. Syed and R. Mogul, Nearly 220 million people in Pakistan without power after countrywide outage; 2023. [online]. Available: <https://edition.cnn.com>.
- [3] K. Yan, G. Li, R. Zhang, Y. Xu, T. Jiang and X. Li, “Frequency Control and Optimal Operation of Low-Inertia Power Systems With HVDC and Renewable Energy: A Review,” *IEEE Trans. Power Syst.*, vol. 39, no. 2, pp. 4279–4295, Mar. 2024.
- [4] L. Meng, J. Zafar, S. K. Khadem, A. Collinson, K. C. Murchie, F. Coffele, and G. M. Burt, “Fast Frequency Response From Energy Storage Systems—A Review of Grid Standards, Projects and Technical Issues,” *IEEE Trans. Smart Grid*, vol. 11, no. 2, pp. 1566–1581, Mar. 2020.
- [5] S. A. Hosseini, M. Toulabi, A. Ashouri-Zadeh, and A. M. Ranjbar, “Battery energy storage systems and demand response applied to power system frequency control,” *Int. J. Electr. Power Energy Syst.*, vol. 136, Mar. 2022, Art. no. 107680.
- [6] A. Bera, B. R. Chalamala, R. H. Byrne and J. Mitra, “Sizing of Energy Storage for Grid Inertial Support in Presence of Renewable Energy,” *IEEE Trans. Power Syst.*, vol. 37, no. 5, pp. 3769–3778, Sept. 2022.
- [7] X. Li and S. Wang, “Energy management and operational control methods for grid battery energy storage systems,” *CSEE J. Power Energy Syst.*, vol. 7, no. 5, pp. 1026–1040, Sept. 2021.
- [8] L. He, Z. Tan, Y. Li, Y. Cao and C. Chen, “A Coordinated Consensus Control Strategy for Distributed Battery Energy Storages Considering Different Frequency Control Demands,” *IEEE Trans. Sustain. Energy*, vol. 15, no. 1, pp. 304–315, Jan. 2024.
- [9] M. Yang, Rapid Growth of New-Type Energy Storage in Jiangsu; 2025. [online]. Available: <https://www.escn.com.cn/news/show-2087343.html>.
- [10] China Energy Storage Network News Center, Asia's Largest Coal-Fired Plant Energy Storage Frequency Regulation Project: Yangxi Plant's 105MW/111.82MWh System Passes Final Inspection; 2025. [online]. Available: <https://www.escn.com.cn/news/show-2120046.html>.
- [11] H. Hui, Y. Ding, Y. Song and S. Rahman, “Modeling and control of flexible loads for frequency regulation services considering compensation of communication latency and detection error,” *Appl. Energy*, vol. 250, pp. 161–174, Sep. 2019.

- [12] N. S. G. E., C. A. Cañizares, K. Bhattacharya, and D. Sohm, "Frequency Regulation Model of Bulk Power Systems With Energy Storage," *IEEE Trans. Power Syst.*, vol. 37, no. 2, pp. 913–926, Mar. 2022.
- [13] H. He, X. Cai, Y. Su, X. Zhang, N. Zhang, S. Ci, Y. Zhou, and C. Kang, "Impact of Communication Time Delay in a 5G Network on Frequency Regulation Performance of a High Renewable Energy Penetrated Power System," *IEEE Internet Things J.*, vol. 11, no. 14, pp. 24376–24388, Jul. 2024.
- [14] Q. -D. Ho, Y. Gao, and T. Le-Ngoc, "Challenges and research opportunities in wireless communication networks for smart grid," *IEEE Wireless Commun.*, vol. 20, no. 3, pp. 89–95, Jun. 2013.
- [15] A. Mahmood, N. Javaid, and S. Razzaq, "A review of wireless communications for smart grid," *Renew. Sustain. Energy Rev.*, vol. 41, pp. 248–260, Jan. 2015.
- [16] P. Mohammad, A. H. Zarif, A. Nouruzi, N. Mokari, M. R. Javan, B. Abbasi, A. Ghasemi, and H. Yanikomeroglu, "Spectrum Sharing Schemes From 4G to 5G and Beyond: Protocol Flow, Regulation, Ecosystem, Economic," *IEEE Open J. Commun. Soc.*, vol. 4, pp. 464–517, Jan. 2023.
- [17] W. K. Alsaedi, H. Ahmadi, Z. Khan and D. Grace, "Spectrum Options and Allocations for 6G: A Regulatory and Standardization Review," *IEEE Open J. Commun. Soc.*, vol. 4, pp. 1787–1812, Aug. 2023.
- [18] *Final Report of 3GPP TSG RAN WG1 Meeting #88 Version 1.0.0 Athens Greece*, Feb. 2017, [online]. Available: <https://www.3gpp.org>.
- [19] Y. Huang, S. Li, C. Li, Y. T. Hou, and W. Lou, "A Deep-Reinforcement-Learning-Based Approach to Dynamic eMBB/URLLC Multiplexing in 5G NR," *IEEE Internet Things J.*, vol. 7, no. 7, pp. 6439–6456, Jul. 2020.
- [20] A. Anand, G. de Veciana, and S. Shakkottai, "Joint Scheduling of URLLC and eMBB Traffic in 5G Wireless Networks," *IEEE/ACM Trans. Netw.*, vol. 28, no. 2, pp. 477–490, Apr. 2020.
- [21] Y. Zhao, X. Chi, L. Qian, Y. Zhu, and F. Hou, "Resource Allocation and Slicing Puncture in Cellular Networks With eMBB and URLLC Terminals Coexistence," *IEEE Internet Things J.*, vol. 9, no. 19, pp. 18431–18444, Oct. 2022.
- [22] F. Rinaldi, A. Raschella, and S. Pizzi, "5G NR system design: A concise survey of key features and capabilities," *Wireless Netw.*, vol. 27, no. 8, pp. 5173–5188, Nov. 2021.
- [23] S. -Y. Lien, S. -L. Shieh, Y. Huang, B. Su, Y. -L. Hsu, and H. -Y. Wei, "5G New Radio: Waveform, Frame Structure, Multiple Access, and Initial Access," *IEEE Commun. Mag.*, vol. 55, no. 6, pp. 64–71, Jun. 2017.



Shaohua Yang (Member, IEEE) is a Postdoctoral Research Associate with the State Key Laboratory of Internet of Things for Smart City, University of Macau, where he received his Ph.D. degree in Electrical and Computer Engineering. His research interests include cyber-physical power systems, control of flexible resources, and power quality, with a special focus on security. One of his papers as the first author was selected as the ESI Hot Paper (Top 0.1%) and two of his papers as the first author was selected as the ESI Highly Cited Paper (Top 1%).

He got the Best Paper Award of IEEE EI2 2023. He also serves as reviewer for many international journals, including IEEE Transactions on Power Systems, IEEE Transactions on Smart Grid, IEEE Transactions on Information Forensics & Security, IEEE Transactions on Control of Network Systems, Applied Energy, etc.



Fen Hou (Member, IEEE) received the PhD degree in electrical and computer engineering from University of Waterloo, Canada in 2008. She is currently an associate professor at State Key Laboratory of IoT for Smart City, Department of Electrical and Computer Engineering, and Guangdong- Hong Kong-Macau Joint Laboratory for Smart Cities, University of Macau, China. Her research interests include resource allocation intelligent computing networks, mechanism design and optimal user behavior in crowd sensing networks, etc. She was a co-recipient of the IEEE Globecom Best Paper Award in 2010, the Distinguished Service Award in the IEEE MMTC in 2011, and the IEEE VTC-Fall Best Student Paper Award in 2021. She served as the TPC chair and co-chair for several IEEE conferences, such as ICCS 2014, INFOCOM 2014, ICCC 2015, ICC 2016, and ICCC 2021. She currently serves as an associate editor of IEEE Transactions on Wireless Communications and IEEE Communications Surveys and Tutorials.



Jian Feng (Graduate Student Member, IEEE) received the B.E. degree from Nanjing Tech University, Nanjing, China, in 2018. He received the M.E. degree in Shenzhen University, Shenzhen, China, in 2023. He is currently working toward the Ph.D. degree in the State Key Laboratory of Internet of Things for Smart City, University of Macau, Macau, China. His research interests include age of information (AoI), resource allocation, and wireless communications in the smart grid.



Hongxun Hui (Senior Member, IEEE) received the B.E. and Ph.D. degrees in electrical engineering from Zhejiang University, Hangzhou, China, in 2015 and 2020, respectively. From 2018 to 2019, he was a Visiting Scholar with the Advanced Research Institute, Virginia Tech, Blacksburg, VA, USA, and also with the CURENT Center, University of Tennessee, Knoxville, TN, USA. He is currently an Assistant Professor with the State Key Laboratory of Internet of Things for Smart City, University of Macau, Macau, China. His research focuses on smart grid optimization and control, demand response, power economics, carbon markets, and interdisciplinary energy-environment systems.